IEEE Access
Multidisciplinary | Rapid Review | Open Access Journal

Received October 30, 2021, accepted November 10, 2021, date of publication November 12, 2021,
date of current version November 19, 2021.

Digital Object Identifier 10.1109/ACCESS.2021.3128050

Dispatchable High-Power Wind Turbine Based on a Multilevel Converter With Modular Structure and Hybrid Energy Storage Integration

GUSTAVO F. GONTIJO[1], (Member, IEEE), DEZSO SERA[2], (Senior Member, IEEE), MATTIA RICCO[3], (Senior Member, IEEE), LASZLO MATHE[4], (Senior Member, IEEE), TAMAS KEREKES[1], (Senior Member, IEEE), AND REMUS TEODORESCU[1], (Fellow, IEEE)

[1]AAU Energy, Aalborg University, 9220 Aalborg East, Denmark
[2]School of Electrical Engineering and Robotics, Queensland University of Technology, Brisbane, QLD 4000, Australia
[3]Department of Electrical, Electronic and Information Engineering, University of Bologna, 40136 Bologna, Italy
[4]Robert Bosch, 1103 Budapest, Hungary

Corresponding author: Gustavo F. Gontijo (gfgo@et.aau.dk)

ABSTRACT This paper presents a new multilevel converter solution with modular structure and hybrid energy-storage integration suitable to drive modern/future high-power medium-voltage wind turbines. The hybrid energy-storage integration means that part of the converter submodules are built with batteries and part of them with conventional capacitors. Since traditional wind turbines are non-dispatchable generators, the integration of an energy storage system could be beneficial in multiple ways as the wind power plant could provide stability support to the grid, improvement of the unit commitment and economic dispatch, and the power plant owner could increase his revenues in the electricity market. The capacitors of the proposed converter are responsible to transfer the power produced by the wind turbine to the grid, and the batteries are only charged/discharged with the mismatch between the power produced by the turbine and the power to be injected into the grid, considering a dispatchable operation where the power injected into the grid is different from the power generated by the turbine. The medium-voltage structure could be an interesting option to overcome problems related to high currents in modern/future high-power wind turbines resulting in more efficient, more compact and lighter solutions. Modular multilevel converters are suitable to handle medium-voltage levels and they allow for a straightforward integration of energy storage systems in a decentralized manner.

INDEX TERMS Energy storage system, modular multilevel converter, wind turbine.

I. INTRODUCTION

The wind power industry is growing at a fast pace and wind turbines (WTs) with increasing power ratings are emerging. High-power WTs can produce a high amount of energy while optimizing structural costs and dimensions [1]–[3]. Conventional WTs are built with a low-voltage structure including generator and power-electronic converter. However, as the power ratings of WTs increase, the current levels increase as well. At a certain point, the high currents become a problem in terms of losses and in terms of the necessity of a heavy, bulky and expensive structure to handle these currents. A medium-voltage WT can be a more cost-effective solution due to the considerably reduced current levels [4]–[6].

As the penetration of wind generation, and of other renewable energy sources, increases, the complexity of the power systems increases as well. WTs are non-dispatchable generators since it is not possible to control the amount of power injected into the grid, which is dependent on the wind availability at the given moment. Besides, these generators are decoupled from the grid through power-electronic converters. Thus, problems related to frequency stability and to a reduced grid inertia emerge. A wind power plant with an integrated energy storage system (ESS) can be beneficial to both the power system operator and the power plant owner. From the grid perspective, the wind power plant with ESS can operate in a dispatchable fashion assisting in the grid

The associate editor coordinating the review of this manuscript and approving it for publication was Fabio Massaro.

frequency regulation and in the economic dispatch [7]–[9]. Besides, control techniques can be applied to the WT so that it presents an inertial response where the power injected into the grid would come from the ESS [8]. Moreover, the ESS can improve the power quality at the point of connection of the wind power plant by reducing the high variability of WT generation and, thus, reducing voltage fluctuations of the weak grid [9]. Finally, wind power plants with an ESS could help in the grid black start, in a bottom-up approach, reducing the restoration time and, thus, reducing the socioeconomic impact of a blackout [10]. The wind power plant owner, on the other hand, could increase his revenues in the electricity market [11] and could provide ancillary services to the grid if the power plant had an integrated ESS.

Converters with a modular multilevel structure are attractive options for medium-voltage applications and they allow for a straightforward integration of ESSs in a decentralized manner in which the ESS devices are distributed among the many submodules of the converter [12]–[16]. If batteries are considered as the ESS, then a large battery system can be integrated into the converter without the necessity of high voltage values. In other words, the medium-voltage level of the application is distributed among the many submodules in such a way that the battery pack integrated into each submodule only needs to deal with a small fraction of the total voltage. This results in battery packs with a reduced number of series-connected cells, which should require a battery management system (BMS) with reduced complexity and, thus, reduced cost.

Recently, a new converter solution with modular multilevel structure and decentralized battery integration used to drive a high-power medium-voltage WT was presented [17]. This converter was named modular multilevel shunt converter (MMShC), and it was presented as an extended version of the topology proposed in the patent [18] for low-voltage residential photovoltaic applications. In [17], the MMShC was presented and validated through both simulation and experimental results. The WT driven by the MMShC could operate in a dispatchable fashion due to the ESS integration. Having the ESS integrated into the same converter that drives the WT avoids the need of an extra converter exclusively dedicated to the ESS. This extra converter would require its own container, control and automation system, cooling system and others. However, the MMShC presented in [17] was built with batteries only. The problem was that these batteries had to deal with the full power of the WT. In other words, the power produced by the WT had to charge the batteries and then these batteries had to be discharged to inject the power into the grid. This way, the lifetime of the batteries was considerably reduced and a large battery system was required.

In this paper, a hybrid version of the MMShC converter is presented as illustrated in Fig. 1, i.e., each submodule string of the hybrid MMShC is built with N full-bridge (FB) submodules with conventional capacitors and with M FB submodules with batteries. The capacitors are responsible for transferring the power produced by the WT to the grid and the batteries are only charged/discharged if there is a surplus power generated by the WT in relation to the grid power set point, or if a power value higher than the instantaneous WT generation must be injected into the grid. It means that the WT is capable to operate in a dispatchable fashion while the battery system is optimized, resulting in a more cost-effective solution. The most common approach to implement an ESS into a wind power plant is to have an extra converter exclusively dedicated to the ESS connected at the point of common coupling of the power plant and the grid [19], [20]. In this traditional solution, the ESS only needs to deal with the mismatch between the power generated by the turbines and the desired power to be injected into the grid. It is important to highlight that this is also the case with the proposed hybrid MMShC, which means that the same ESS dimensions would be required in both cases. However, in the proposed hybrid MMShC, the ESS is integrated into the same converter that drives the WT, which avoids the need of an extra converter exclusively dedicated to the ESS, probably resulting in reduced costs, volume and weight.

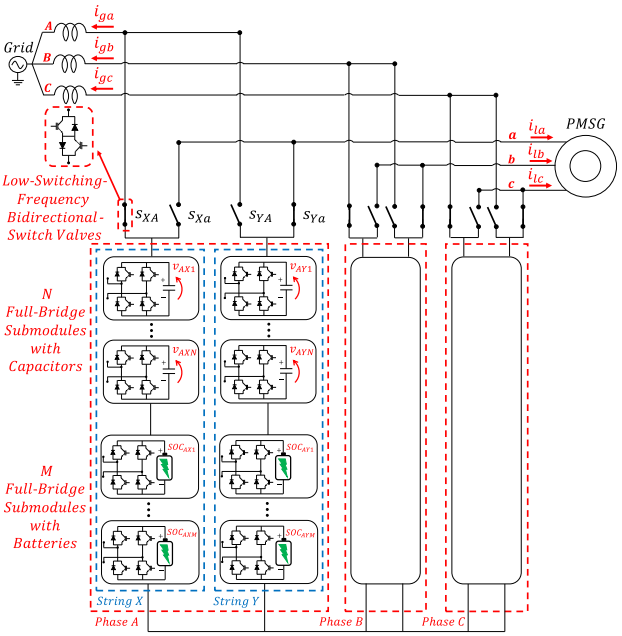

FIGURE 1. Hybrid MMShC.

II. CONVERTER OPERATION

As illustrated in Fig. 1, each MMShC phase is composed of two strings of FB submodules (String X and String Y) along with four bidirectional-switch valves (S_{XA}, S_{Xa}, S_{YA} and S_{Ya}) that are used to connect each string to both grid and generator terminals. These submodule strings operate in a complementary fashion, meaning that while one is connected to the generator, charging, the other is connected to the grid, discharging. This way, a continuous power flow between the generator and the grid is maintained. When the MMShC is

built with integrated batteries only, the bidirectional-switch valves can operate with an extremely low switching frequency, in a scale of several minutes. In the hybrid MMShC, however, the bidirectional-switch valves must switch faster since the conventional capacitors are the ones being charged and discharged with the majority of the WT power. Nonetheless, as will be demonstrated in this paper, the bidirectional-switch valves can still operate with a low switching frequency (between 5 Hz and 100 Hz) even in the hybrid solution. Since the MMShC is proposed for medium-voltage WTs, then the bidirectional-switch valves might need to be built with series-connected semiconductor devices. Nonetheless, since these are medium-voltage levels and not high-voltage ones, then only a few series-connected switches would be required, especially considering the availability of modern devices with voltage ratings of up to 6.5 kV and some devices with voltage ratings of up to 10 kV under test. Several series-connected semiconductor devices operating with high switching frequency is a challenge due to problems with static and dynamic voltage sharing among the series-connected switches [21], [22]. This problem can be non-existent or at least can be considerably reduced when only a few switches are connected in series and when these devices operate with low switching frequency, which is the case of the bidirectional-switch valves of the proposed MMShC. There are some products currently available in the industry that are valves composed of many series-connected semiconductor devices and that operate in a safe and reliable fashion due to modern drivers that ensure static and dynamic voltage sharing among the series-connected switches [22]. These valves could be used to build the MMShC bidirectional-switch valves.

The basic operation of the MMShC, no matter if it is built with batteries, with capacitors or in a hybrid manner, is illustrated in Fig. 2. String X and String Y essentially behave as controlled voltage sources, that can be connected to both grid and generator terminals, synthesizing a voltage profile according to a given reference. The converter operates switching between State 1 and State 2 as illustrated in Fig. 2. In State 1, String Y is connected to the generator terminals and it is charged with the WT power (P_{la}) while controlling the generator speed. Meanwhile, String X is connected to the grid terminals and it injects into the grid a power value (P_{ga}), which not necessarily needs to be equal to the power produced by the WT. If the MMShC has an integrated ESS, then the WT can operate in a dispatchable fashion injecting the desired power into the grid. State 2 is the opposite of State 1, i.e., String Y is connected to the grid terminals and it is discharged with a power value equal to (P_{ga}), while String X is connected to the generator terminals and it is charged with the WT power (P_{la}). The MMShC converter switches between State 1 and State 2 through the operation of the bidirectional-switch valves. In this paper, the switching frequency of the bidirectional-switch valves is kept fixed with a value equal to 5 Hz as will be explained later in this work. It means that, every $\frac{1}{5\text{Hz}} = 0.2$ s, the MMShC changes from State 1 to State 2 or vice versa. This is obviously a quite low switching frequency for the bidirectional-switch valves.

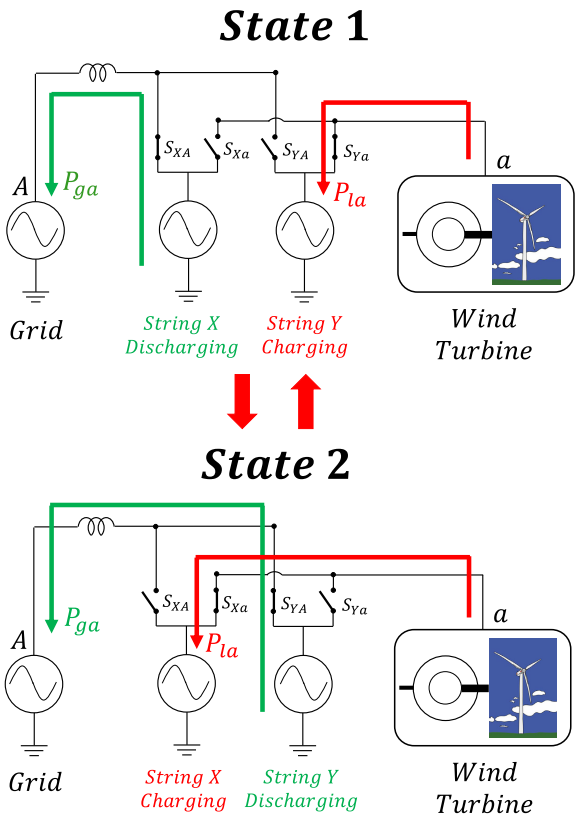

FIGURE 2. MMShC basic operation.

In order to explain the operation of the hybrid MMShC, let us suppose an hypothetical example as illustrated in Fig. 3. At the given moment described in this example, String Y is connected to the generator terminals and it absorbs a power from the WT equal to 4 MW with a 1-kA current. Moreover let us consider that, at the given moment, four submodules must be inserted to synthesize the desired instantaneous voltage at the generator terminals. String X, on the other hand, is connected to the grid terminals and it is controlled to inject a power value into the grid equal to 4 MW with a 1-kA current. Similarly to String Y, let us suppose that at the given moment four submodules must be inserted to synthesize the desired voltage at the grid terminals. Considering that all submodule capacitors of both strings should be regulated with an average value equal to 1 kV, then, in this example, each submodule capacitor of each string will be charged/discharged with a power value equal to 1 MW. Thus, it means that the capacitors of String Y will be charged with the same amount of power (same rate) that the capacitors of String X will be discharged. In other words, considering that the submodule capacitors of both strings present equal capacitance, then the increase of the voltage value of the submodule capacitors connected to the generator terminals will be equal to the

reduction of the voltage value of the submodule capacitors connected to the grid terminals.

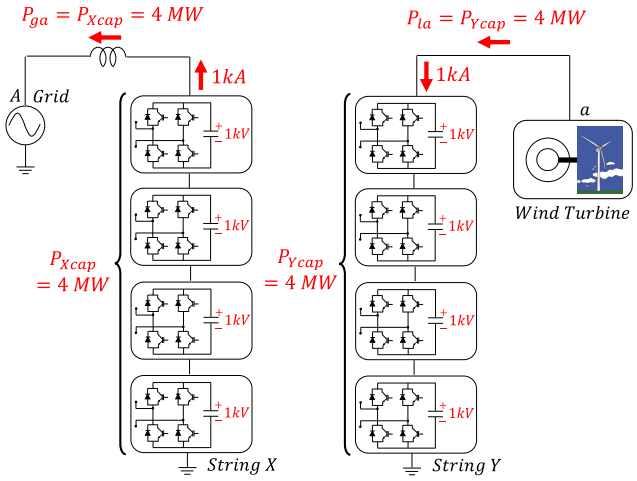

FIGURE 3. Power generated by WT equal to power injected into the grid.

Let us now suppose that the system operates in a dispatchable manner in which the instantaneous power that is injected into the grid is higher (8 MW) than the instantaneous power generated by the WT (4 MW). This operation mode is illustrated in Fig. 4.

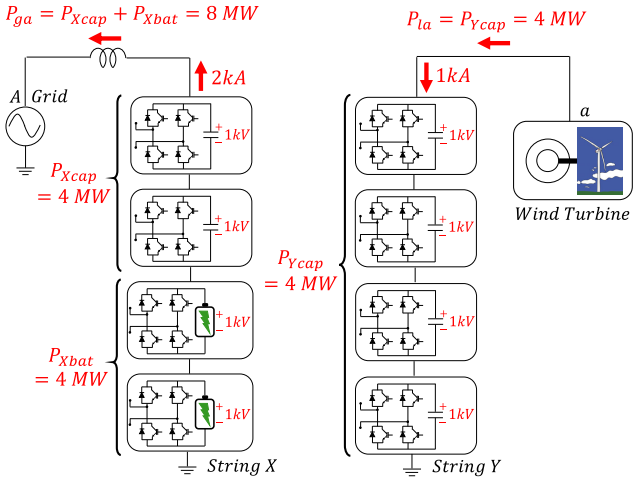

FIGURE 4. Power generated by WT lower than power injected into the grid.

Similarly to the previous example, at the given moment, String Y is connected to the generator terminals and it extracts a power from the WT equal to 4 MW with a 1-kA current. Moreover, at the given moment, four submodules must be inserted to synthesize the desired voltage at the generator terminals. String X, on the other hand, is connected to the grid terminals and it needs to inject into the grid 8 MW with a 2-kA current, but the instantaneous number of submodules to be inserted to synthesize the desired voltage is also equal to four. In this case, if two submodules with capacitors are inserted and two submodules with batteries are inserted, then each capacitor inserted will be discharged with 2 MW and each battery inserted will also be discharged with 2 MW. It is interesting to notice that String X will be injecting into the grid 8 MW but its capacitors will only be discharged with 4 MW, which is the same amount of power with which the capacitors of String Y will be charged. The batteries will inject into the grid only the extra power value required to meet the grid power set point. In other words, the increase of the voltage value of the submodule capacitors connected to the generator terminals will still be equal to the reduction of the voltage value of the submodule capacitors connected to the grid terminals, which is the same that happened in the previous example (illustrated in Fig. 3), in which the power injected into the grid was equal to the power produced by the WT.

Finally, let us consider the case in which the power that must be injected into the grid (power set point) is lower than the power instantaneously generated by the WT. This situation is illustrated in Fig. 5 and the power to be injected into the grid is equal to 2 MW, while the power produced by the WT is equal to 4 MW. String X will inject 2 MW into the grid with a 0.5-kA current and four submodules will be inserted to synthesize the desired instantaneous voltage at the grid terminals. Each String-X capacitor will be discharged with 0.5 MW and the total power supplied by the four capacitors will be equal to 2 MW. String Y will absorb 4 MW from the WT with a 1-kA current. In order to charge the String-Y capacitors with the same power as the String-X capacitors will be discharged, then two submodules with capacitors and two submodules with batteries will be inserted, since it is once again supposed that four submodules must be inserted to synthesize the desired instantaneous voltage at the generator terminals. As illustrated in Fig. 5, String Y will absorb 4 MW from the WT but the capacitors will only be charged with 2 MW, which is the same power with which the String-X capacitors will be discharged. The surplus power generated by the WT will be stored in the batteries. Once again, the increase of the voltage value of the submodule capacitors connected to the generator terminals will also be equal to the reduction of the voltage value of the submodule capacitors connected to the grid terminals, which is the same that happened in the two previous examples.

Obviously, the explanation provided through Fig. 3, Fig. 4 and Fig. 5 is a simplified version of the real operation of the proposed solution, however it helps in the comprehension of the converter behavior. The average value of the MMShC capacitor voltages must be kept constant and regulated for the proper operation of the converter. In theory, if the power injected into the grid by the converter is controlled to be equal to the power absorbed from the WT, then the average value of the capacitor voltages could be kept constant since the capacitors of the string connected to the generator would always be charged with the same amount of power that the capacitors of the string connected to the grid terminal would be discharged (same charging/discharging rates).

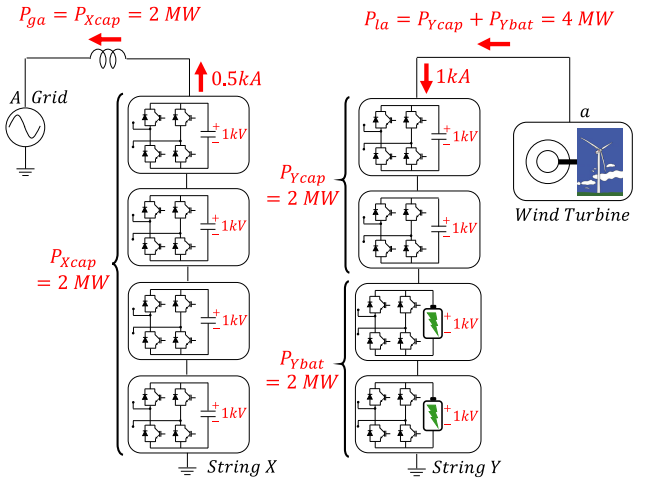

FIGURE 5. Power generated by WT higher than power injected into the grid.

Since a dispatchable operation is considered, then there will be a mismatch between the instantaneous power generated by the WT and the instantaneous power to be injected into the grid. Thus, the regulation of the submodule-capacitor voltages can be achieved by controlling the instantaneous number of battery submodules inserted in such a way as to always maintain an equal power value discharging the submodule capacitors of the string connected to the grid and charging the submodule capacitors of the string connected to the generator. The extra power is absorbed/supplied by the batteries. This control approach was exemplified in Fig. 3, Fig. 4 and Fig. 5 in which the increase and reduction of the voltages in the charging and discharging capacitors were kept equal no matter if the power injected into the grid was equal, higher or lower than the power generated by the WT, which means that the average value of the submodule-capacitor voltages would always remain constant and regulated. If the power to be injected into the grid is higher than the power instantaneously produced by the WT, then as higher the mismatch, more battery submodules and less capacitor submodules must be inserted in the string connected to the grid terminal at the given moment. On the other hand, if the power instantaneously produced by the WT is higher than the power to be injected into the grid, then as higher the mismatch, more battery submodules and less capacitor submodules must be inserted in the string connected to the generator terminal at the given moment. This operation will be further explained through a flowchart and with simulation results later in this work.

III. SIMULATION ANALYSIS

To validate the proposed hybrid MMShC illustrated in Fig. 1, simulations based on the software PSCAD/EMTDC will be presented. In these simulations, each string of the hybrid MMShC is built with $N = 5$ FB submodules with capacitors (50 mF) and with $M = 4$ FB submodules with batteries. The batteries have rated voltage equal to 1 kV and energy value equal to 65 mAh. The converter is connected to a 5-kV, 50-Hz grid and it drives a permanent-magnet synchronous generator (PMSG) that represents the WT. This is a 3-MVA generator. The power injected into the grid by the converter (P_g) is controlled in an open-loop fashion by simply varying the phase of the voltage synthesized at the grid terminals. The generator speed and power is controlled through a field-oriented control (FOC).

A. CONVERTER WITH CAPACITORS ONLY

The first simulation aims to explain the operation of the converter if the batteries remained in stand-by mode and only the submodules with capacitors were used in the converter operation. The simulation results are shown in Fig. 6.

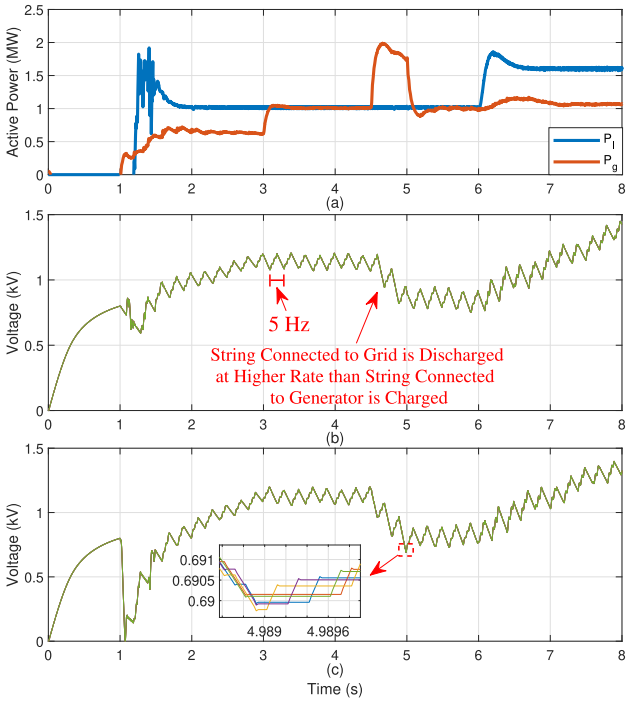

FIGURE 6. (a) Grid-side and generator-side power; (b) Phase-A String-*X* submodule-capacitor voltages and (c) Phase-A String-*Y* submodule-capacitor voltages.

The MMShC grid-side power (P_g) and generator-side power (P_l) are controlled to assume different values during the simulation period (see Fig. 6(a)). During some moments, the grid-side power is kept lower than the generator-side power, during some moments the grid-side power is kept higher than the generator-side power and during some moments the grid-side power and the generator-side power are kept with equal values. In Fig. 6(b) and (c), the MMShC phase-A String-*X* and phase-A String-*Y* submodule-capacitor voltages are shown, respectively. Fig. 6(b) is interesting because it is capable to explain the basic operation of the MMShC in an intuitive way. It is clear that the submodule capacitor voltages present a ripple with a 5-Hz frequency. This ripple is a consequence of the operation of the bidirectional-switch valves that are connecting the

submodule string to the grid and to the generator terminals every $\frac{1}{5\text{Hz}} = 0.2$ s. Since Fig. 6(b) shows the String-X submodule-capacitor voltages, then the moments in which the voltage is decreasing correspond to State 1 of Fig. 2, which means that String X is connected to the grid terminals and it is discharging. The moments in which the voltage is increasing correspond to State 2 of Fig. 2, which means that String X is connected to the generator terminals and it is charging. The amplitude of the submodule-capacitor voltage ripple is a function of the power values charging/discharging the capacitors, of the switching frequency of the bidirectional-switch valves and of the capacitor capacitance value. For example, if the switching frequency of the bidirectional-switch valves was reduced to 1 Hz, then the capacitors of the string connected to the grid would discharge five times more before the string was connected to the generator terminal and the capacitors of the string connected to the generator would charge five times more before the string was connected to the grid terminal. In other words, a higher ripple would occur. It is interesting to notice that the voltage ripple shown in Fig. 6(b) is quite small for an extremely low switching frequency (5 Hz). It is true that the submodule-capacitor capacitance adopted in this paper was considerably big (50 mF). Nonetheless, even if smaller capacitors were adopted (5-10 mF), a low ripple could still be obtained by increasing the switching frequency of the bidirectional-switch valves to values between 25 Hz and 50 Hz. These are still very low switching frequencies.

Another fact that is important to notice in Fig. 6(b) and Fig. 6(c) is that the average value of the submodule-capacitor voltages is kept constant when the power injected into the grid (P_g) is equal to the power extracted from the WT (P_l). This is because the capacitors are being charged and discharged at the same rate. Between $t = 4.5$ s and $t = 5$ s, the power injected into the grid becomes considerably higher than the power extracted from the WT and, thus, the average value of the submodule-capacitor voltages decreases. That is because when the strings are connected to the grid terminals, they are discharged at a higher rate than they are charged when they are connected to the generator terminals. On the contrary, when the power extracted from the WT is higher than the power injected into the grid, after $t = 6$ s for example, then the average value of the submodule-capacitor voltages increases since the capacitors of the strings connected to the generator terminals are charged at a higher rate than the capacitors of the strings connected to the grid terminals are discharged. In order for the WT solution to operate in a dispatchable fashion while maintaining the submodule-capacitor voltages regulated, then the insertion of submodules with batteries is necessary. Finally, another important issue to observe in Fig. 6(c) is the zoom in the voltage signals that shows that the five capacitors within the same string remain with similar voltage values due to a sorting algorithm responsible for the voltage-balancing control. This algorithm will be explained later in this paper.

B. IDEAL OPERATION

In this subsection, simulation results will be presented to demonstrate how it is possible to operate the WT solution in a dispatchable fashion while maintaining the submodule-capacitor voltages regulated and with the submodule batteries absorbing/supplying the mismatch between the power injected into the grid and the power produced by the WT. The MMShC strings are built with $N = 5$ FB submodules with capacitors, which means that a 11-level voltage can be synthesized by the converter. In other words, the instantaneous number of submodules to be inserted (Z) to synthesize the desired voltage varies between 0 and 5 and these submodules can be inserted with both positive and negative polarities since FB submodules are used. Let us suppose that, at a given moment, the instantaneous number of submodules to be inserted to obtain the desired voltage at the grid terminals is equal to $Z = 4$. The same instantaneous voltage can be synthesized if different combinations of submodules with capacitors and with batteries are inserted considering that the capacitors and batteries have equal nominal voltages. For example, the number of submodules with capacitors inserted could be equal to $N_{cap} = 4$ and the number of submodules with batteries inserted could be equal to $N_{bat} = 0$. Another possibility would be to insert $N_{cap} = 3$ capacitor submodules and $N_{bat} = 1$ battery submodule. Or insert $N_{cap} = 2$ capacitor submodules and $N_{bat} = 2$ battery submodules. In all the cases, the same instantaneous voltage would be synthesized at the grid terminals but the string capacitors and batteries would be discharged at different rates. In the first example, only the string capacitors would be discharged to supply power to the grid, while in the last case, the string capacitors and batteries would be sharing equally the power injected into the grid. With this approach, it is possible to maintain a balance between the power absorbed by the capacitors of the submodule string connected to the generator terminals and the power supplied by the capacitors of the submodule string connected to the grid terminals. In other words, the average value of the submodule-capacitor voltages can be regulated by controlling the insertion of submodules with batteries. In this subsection, an ideal operation is demonstrated in which the power absorbed/supplied by the batteries through the insertion of a fixed number of battery submodules is exactly equal to the surplus power either injected into the grid or absorbed from the WT. The simulation results shown in Fig. 7 can provide a clear and intuitive explanation of this ideal operation. The realistic operation case will be presented in the next subsection.

In Fig. 7(a) and (b), the voltages synthesized by the hybrid MMShC at the grid and generator terminals are shown, respectively. As expected, these are 11-level voltages. In Fig. 7(c), the grid-side power (P_g) and generator-side power (P_l) are shown. Similarly to the previous simulation, the grid-side and generator-side power values vary along the simulation period and sometimes the grid-side power is higher than the generator-side power and sometimes the

generator-side power is higher than the grid-side power. In Fig. 7(d), the generator angular speed is shown, which is regulated with a fixed value equal to 0.22 pu during the entire simulation period. In Fig. 7(e) and (f), the phase-A String-X submodule-capacitor voltages and phase-A String-Y submodule-capacitor voltages are shown, respectively. In Fig. 7(g) and (h), the phase-A String-X submodule-battery state of charge (SOC) and phase-A String-Y submodule-battery SOC are shown, respectively. At $t = 1$ s, the system start-up occurs and from $t = 1$ s until $t = 2.7$ s, the power injected into the grid is regulated with a value lower than the power generated by the WT in such a way that the submodule capacitors are charged until they reach their nominal voltage equal to 1 kV. During the start-up procedure, the battery submodules are kept by-passed. At $t = 2.7$ s, the power injected into the grid is regulated to assume a value equal to the power being produced by the WT in such a way that the submodule-capacitor voltages are kept constant with 1 kV, i.e., the capacitors of the strings connected to the grid are discharged at the same rate as the capacitors of the strings connected to the generator are charged.

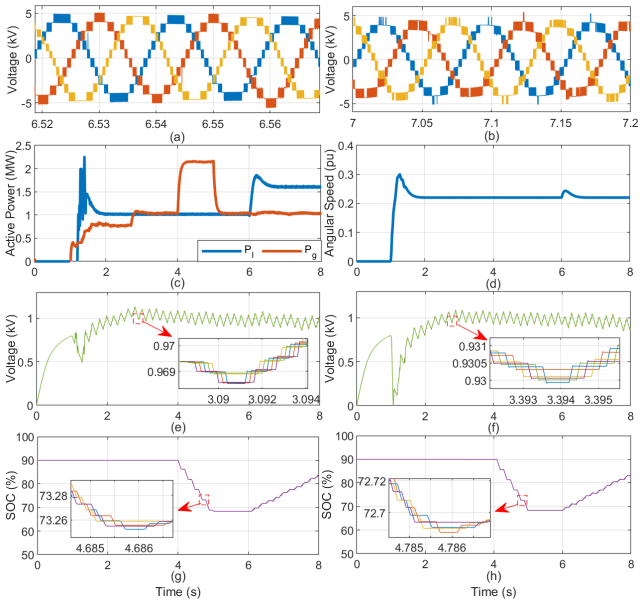

FIGURE 7. (a) Voltages synthesized at grid terminals; (b) voltages synthesized at generator terminals; (c) grid-side and generator-side power; (d) generator speed; (e) phase-A String-X submodule-capacitor voltages; (f) phase-A String-Y submodule-capacitor voltages; (g) phase-A String-X submodule-battery SOC and (h) phase-A String-Y submodule-battery SOC.

At $t = 4$ s, the power injected into the grid (P_g) becomes considerably higher than the power generated by the WT (P_l). The power mismatch between P_g and P_l in this case was set intentionally to a given value that corresponds exactly to the necessity of inserting two battery submodules in the strings connected to the grid terminal in such a way as to maintain the regulation of the submodule-capacitor voltages. In this case, when the submodule string is connected to the generator terminals, then only submodules with capacitors must be inserted, i.e., $N_{cap} = Z$, which means that the instantaneous number of capacitor submodules to be inserted is equal to the instantaneous number of submodules that must be inserted to synthesize the desired voltage at the generator terminals. When the submodule string is connected to the grid, however, then the procedure to insert submodules is as follows: if $Z \leq 2$, then $N_{cap} = 0$ and $N_{bat} = Z$. If $Z > 2$, then $N_{cap} = Z - 2$ and $N_{bat} = 2$. In other words, the submodules with batteries are inserted with priority and if the instantaneous number of submodules to be inserted is at least equal to $Z = 2$, then always $N_{bat} = 2$ battery submodules must be inserted and the rest of submodules to be inserted to reach the instantaneous value of Z are capacitor submodules. In Fig. 7(g) and (h), it is possible to notice that the battery-SOC values of both submodule strings are kept constant before $t = 4$ s, since only capacitor submodules are inserted. At $t = 4$ s, the battery-SOC values of both strings start to decrease as the battery submodules start to be inserted as previously explained. It is very interesting to notice that the submodule-capacitor voltages are kept constant, which means that the capacitors of the strings connected to the grid are being discharged at the same rate as the capacitors of the strings connected to the WT are being charged. The surplus power injected into the grid is coming from the energy stored in the batteries. At $t = 5$ s, the power injected into the grid is reduced and it becomes again equal to the power produced by the WT. Thus, only submodules with capacitors need to be inserted and all the submodules with batteries are kept by-passed. In Fig. 7(g) and (h), it is clear that the battery SOC values become constant again at $t = 5$ s, since the submodules with batteries are kept by-passed as they don't need to be inserted anymore since $P_g = P_l$.

At $t = 6$ s, the mechanical torque of the WT is increased, representing a step in the wind speed, and the power generated by the WT becomes higher than the power injected into the grid. In this case, every time a submodule string is connected to the generator terminals, then submodules with batteries must be inserted to absorb the surplus power generated by the WT in order to preserve the balance between the power being injected into the grid by the submodule capacitors and the power absorbed from the WT by the submodule capacitors. This way, the average value of the submodule-capacitor voltages is kept constant and regulated. The power mismatch between P_g and P_l in this case was set intentionally to a given value that corresponds exactly to the necessity of inserting one battery submodule in the strings connected to the generator terminal in such a way as to maintain the regulation of the submodule-capacitor voltages. In Fig. 7(c), it is possible to notice that the power mismatch between P_g and P_l in this case is approximately half of the mismatch between the two power values when P_g was higher than P_l (between $t = 4$ s until $t = 5$ s). In that case two battery submodules were necessary and that is why in this case, only one battery submodule is necessary. Since P_l is higher than P_g, then when the submodule string is connected to the grid terminals, only submodules with capacitors must be inserted,

i.e., $N_{cap} = Z$. When the submodule string is connected to the generator, however, then the procedure to insert submodules is as follows: if $Z \leq 1$, then $N_{cap} = 0$ and $N_{bat} = Z$. If $Z > 1$, then $N_{cap} = Z - 1$ and $N_{bat} = 1$. In other words, the submodules with batteries are inserted with priority and if the instantaneous number of submodules to be inserted is at least equal to $Z = 1$, then always $N_{bat} = 1$ battery submodule must be inserted and the rest of submodules to be inserted to reach the instantaneous value of Z are capacitor submodules. In Fig. 7(g) and (h), it is possible to notice that, at $t = 6$ s, the battery-SOC values of both strings start to increase since the battery submodules start to be inserted as previously explained. Once again, it is very interesting to notice that the submodule-capacitor voltages are kept constant, which means that the capacitors of the strings connected to the grid are being discharged at the same rate as the capacitors of the strings connected to the WT are being charged. The surplus power produced by the WT is being stored in the batteries. Another interesting issue to notice in Fig. 7(g) and (h) is that the batteries are discharged at a higher rate between $t = 4$ s and $t = 5$ s than they are charged between $t = 6$ s and $t = 8$ s. This is because, between $t = 4$ s and $t = 5$ s, the mismatch between P_g and P_l is higher and two battery submodules are always inserted if the instantaneous value of Z is at least equal to two. However, between $t = 6$ s and $t = 8$ s, the mismatch between P_g and P_l is lower and only one battery submodule is always inserted if the instantaneous value of Z is at least equal to one. Finally, by observing the zoom in the capacitor-voltage signals and battery-SOC signals in Fig. 7(e), (f), (g) and (h), one can notice the balance of the capacitor voltages and battery SOC of the submodules within the same string. This is a consequence of the sorting algorithm that will be explained later in this paper.

C. CONTROL FOR REALISTIC OPERATION CONDITION

In the previous subsection, the mismatches between the power produced by the WT and the power injected to the grid were set intentionally to given values in which a fixed number of battery submodules had to be inserted to maintain the submodule-capacitor voltages constant and regulated. When P_g was higher than P_l, then the insertion pattern of battery submodules was the following: when the submodule string was connected to the grid, if $Z \leq 2$, then $N_{cap} = 0$ and $N_{bat} = Z$. If $Z > 2$, then $N_{cap} = Z - 2$ and $N_{bat} = 2$. In other words, a fixed number of submodules with batteries (equal to $N_{bat} = 2$) was always inserted if the instantaneous value of Z was at least equal to $Z = 2$. When P_g was lower than P_l, on the other hand, then the insertion pattern of battery submodules was the following: when the submodule string was connected to the generator, if $Z \leq 1$, then $N_{cap} = 0$ and $N_{bat} = Z$. If $Z > 1$, then $N_{cap} = Z - 1$ and $N_{bat} = 1$. In other words, a fixed number of submodules with batteries (equal to $N_{bat} = 1$) was always inserted if the instantaneous value of Z was at least equal to $Z = 1$. In both cases, the power supplied/absorbed by the submodules with batteries was exactly equal to the mismatch between P_g and P_l. This was an ideal operation condition intentionally imposed to explain the operation of the hybrid MMShC in a didactic and intuitive fashion. In reality, the power mismatch between P_g and P_l will be constantly varying and the power supplied/absorbed by the batteries if a fixed number of battery submodules are inserted will rarely be identical to the power mismatch between P_g and P_l. It means that the number of battery submodules to be inserted to keep the submdoule-capacitor voltages constant and regulated must change along time. The simulation results shown in Fig. 8 are capable to explain in a clear and comprehensive way the real operation of the hybrid MMShC. Moreover, a detailed explanation of the control adopted in this simulation is illustrated in the flowchart shown in Fig. 9.

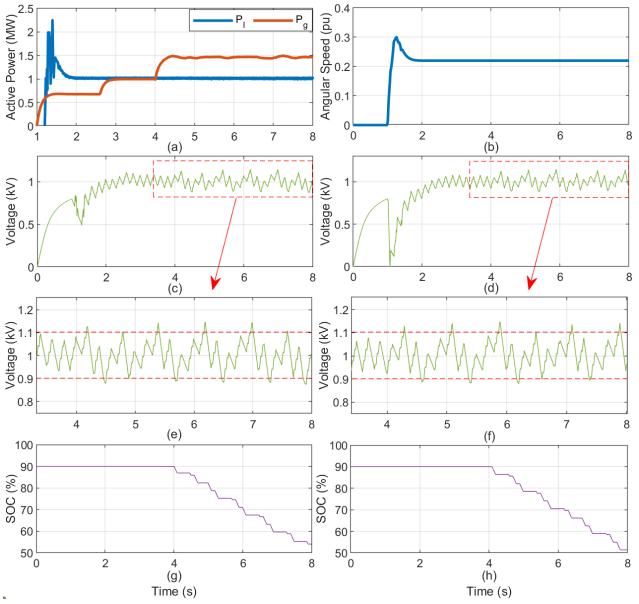

FIGURE 8. (a) Hybrid MMShC grid-side and load-side power values; (b) generator angular speed; (c) phase-A String-*X* submodule-capacitor voltages; (d) phase-A String-*Y* submodule-capacitor voltages; (e) zoom of Fig. 8(c); (f) zoom of Fig. 8(d); (g) phase-A String-*X* submodule-battery SOC and (h) phase-A String-*Y* submodule-battery SOC.

In Fig. 8(a), the power injected into the grid (P_g) and the power absorbed from the WT (P_l) by the hybrid MMShC are shown. In Fig. 8(b), the generator speed is shown and it is kept regulated with a constant value during the entire simulation period. In Fig. 8(c) and (d), the MMShC phase-A String-X submodule-capacitor voltages and phase-A String-Y submodule-capacitor voltages are shown, respectively. From the begining of the simulation until $t = 2.7$ s, the power injected into the grid is kept lower than the power absorbed from the WT so that the submodule capacitors are charged until they reach their nominal voltage equal to 1 kV. At $t = 2.7$ s, the power injected into the grid is regulated to a value equal to the power absorbed from the WT so that the submodule-capacitor voltages are kept constant. At $t = 4$ s, a new set point is given to the power that must be injected into the grid by the hybrid MMShC and, thus, the converter starts to inject into the grid a power

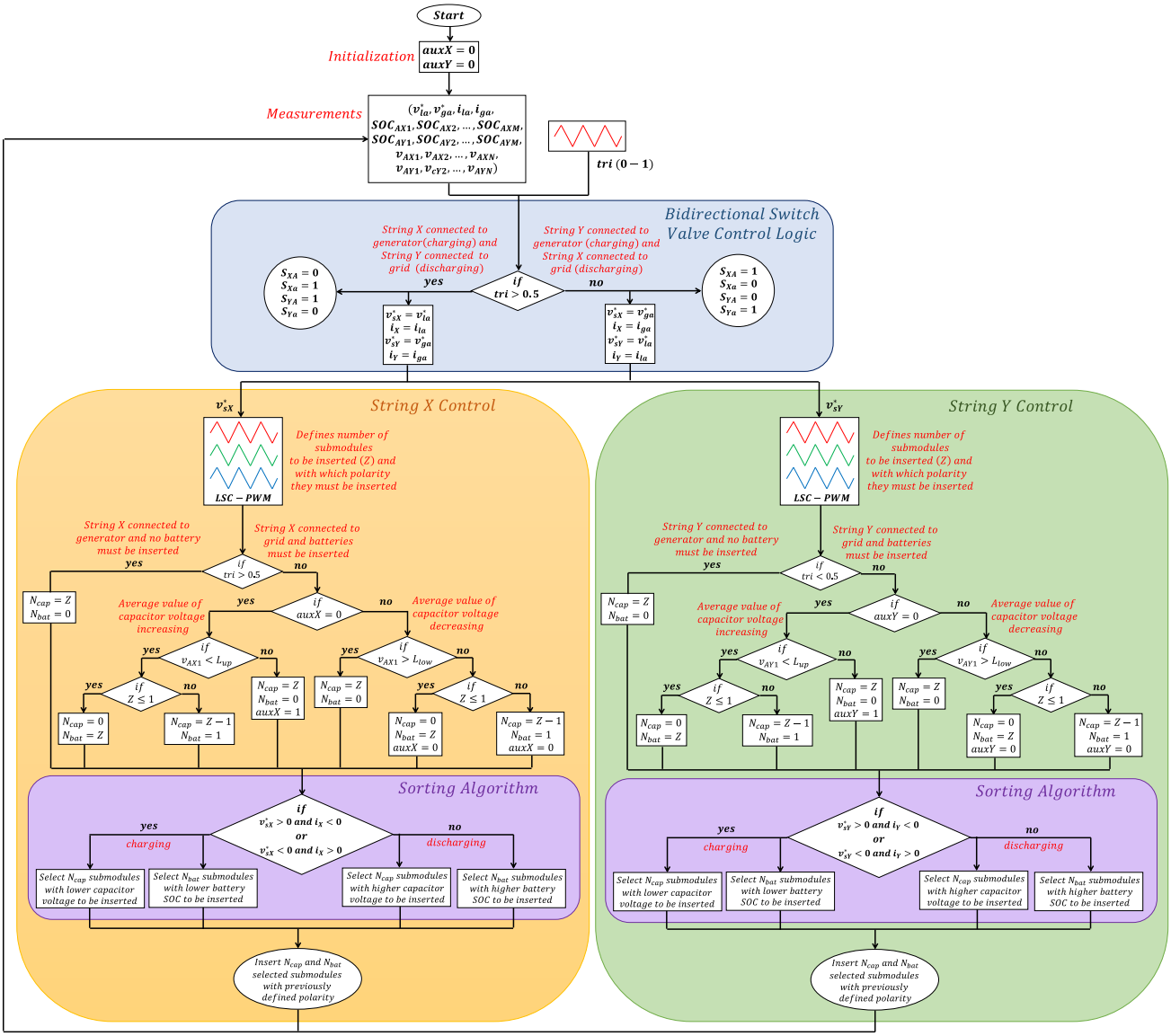

FIGURE 9. Flowchart illustrating a reduced version of the hybrid-MMShC control, which was used to obtain the specific simulation results shown in Fig. 8.

value higher than the power produced by the WT. Then, as previously explained, when a given submodule string is connected to the grid, battery submodules must be inserted to supply the surplus power in such a way as to preserve the balance between the power absorbed by the submodule capacitors when connected to the generator terminals and the power supplied by the submodule capacitors when connected to the grid terminals. However, in this case, the power mismatch presents a value that is obviously higher than the power supplied by the batteries if no battery submodule is inserted, but lower than the power supplied by the batteries if one battery submodule is inserted. Thus, the insertion of battery submodules will have to vary between these two conditions in order to maintain the submodule-capacitor voltages regulated within a limited range. By observing Fig. 8(c) and (d), as well as Fig. 8(e) and (f) (which are zooms of Fig. 8(c) and (d), respectively), one can understand the operation of the hybrid MMShC. At $t = 4$ s, battery submodules start to be inserted when either String X or String Y is connected to the grid terminals. Initially, one battery submodule is inserted, which means that the insertion procedure is as follows: when the submodule string is connected to the grid, if $Z \leq 1$, then $N_{cap} = 0$ and $N_{bat} = Z$. If $Z > 1$, then $N_{cap} = Z - 1$ and $N_{bat} = 1$. However, in this case, the power supplied to the grid by the batteries is higher than the power mismatch between P_g and P_l, which means that the power supplied to the grid by the submodule capacitors is lower than the power absorbed from the WT by the submodule capacitors. Thus, the average value of the submodule-capacitor voltages starts to increase. When the capacitor voltages reach a pre-defined upper limit

equal to 1.1 kV in this case, then the insertion procedure of battery submodules changes to: when the submodule string is connected to the grid, then only capacitor submodules must be inserted, which means that $N_{cap} = Z$ and $N_{bat} = 0$. However, in this case, the power supplied to the grid by the batteries is obviously lower than the power mismatch between P_g and P_l, which means that the power supplied to the grid by the submodule capacitors will be higher than the power absorbed from the WT by the submodule capacitors. Thus, the average value of the submodule-capacitor voltages starts to decrease. When the capacitor voltages reach a pre-defined lower limit equal to 0.9 kV in this case, then the insertion procedure of battery submodules changes back to: when the submodule string is connected to the grid, if $Z \leq 1$, then $N_{cap} = 0$ and $N_{bat} = Z$. If $Z > 1$, then $N_{cap} = Z - 1$ and $N_{bat} = 1$. In this case, the converter must operate varying between the two mentioned conditions. By observing the submodule-capacitor voltages in Fig. 8, it is clear that the regulation of the average value of these voltages can be achieved by controlling the number of inserted battery submodules. In Fig. 8(g) and (h), the MMShC phase-A String-X submodule-battery SOC and phase-A String-Y submodule-battery SOC are shown, respectively. At $t = 4$ s, the battery SOC of both strings start to decrease, as expected, due to the insertion of battery submodules since the power injected into the grid is higher than the power produced by the WT. It is interesting to notice that from $t = 4$ s until the end of the simulation, the batteries are being discharged in average, supplying power to the grid. However, even during this period, there are moments in which the battery SOC decreases and moments in which the battery SOC is kept constant (steps can be observed). The moments in which the battery SOC decreases correspond to the instants in which the corresponding submodule string is connected to the grid and battery submodules are being inserted. The moments in which the battery SOC is kept constant occur in two different situations: either if the submodule string is connected to the generator terminal (in which battery submodules are never inserted since $P_g > P_l$) or if the submodule string is connected to the grid and only capacitor submodules are inserted (moments in which the submodule-capacitor voltages are decreasing before they reach the limit equal to 0.9 kV).

A detailed explanation of the hybrid MMShC phase-A control is shown in Fig. 9. This is a reduced version of the complete converter control, which was used to obtain the specific simulation results shown in Fig. 8. The control shown in the flowchart was implemented in a C code and it was also used for the other two phases of the converter. The control receives as inputs the following signals measured in the simulation: the generator-terminal and grid-terminal voltage references (v^*_{la} and v^*_{ga}, respectively), which come from outer control loops, the currents measured at the generator and grid terminals (i_{la} and i_{ga}, respectively), the battery SOC of the submodules of both strings ($SOC_{AX1}, SOC_{AX2}, \ldots SOC_{AXM}$ and $SOC_{AY1}, SOC_{AY2}, \ldots SOC_{AYM}$) and, finally, the capacitor voltages of the submodules of both strings ($v_{AX1}, v_{AX2}, \ldots v_{AXN}$ and $v_{AY1}, v_{AY2}, \ldots v_{AYN}$). Besides, the control receives as an input a triangular signal (*tri*) with amplitude varying between 0 and 1 and with frequency equal to 5 Hz. This is the signal used to control the switching of the bidirectional-switch valves.

The first step of the control is the bidirectional-switch valve operation logic. Basically, if the triangular signal *tri* is bigger than 0.5, then String X should be connected to the generator terminal (charging mode) and String Y should be connected to the grid terminal (discharging mode). On the contrary, if the triangular signal *tri* is smaller than 0.5, then String X should be connected to the grid terminal (discharging mode) and String Y should be connected to the generator terminal (charging mode). Since the triangular signal has a frequency of 5 Hz, then it means that the bidirectional-switch valves switch with this frequency and, every $\frac{1}{5\text{Hz}} = 0.2$ s, the submodule strings are connected to a different terminal. So, if the triangular signal *tri* is bigger than 0.5, then the bidirectional-switch valves receive the signals $S_{XA} = 0$, $S_{Xa} = 1$, $S_{YA} = 1$, and $S_{Ya} = 0$, in which 1 means ON state and 0 means OFF state. Besides, since String X will be connected to the generator terminal, then the voltage to be synthesized across String X becomes equal to the generator voltage reference ($v^*_{sX} = v^*_{la}$) and the String-X current becomes equal to the generator current ($i_X = i_{la}$). Finally, since String Y will be connected to the grid terminal, then the voltage to be synthesized across String Y becomes equal to the grid voltage reference ($v^*_{sY} = v^*_{ga}$) and the String-Y current becomes equal to the grid current ($i_Y = i_{ga}$). On the contrary, if the triangular signal *tri* is smaller than 0.5, then the bidirectional-switch valves receive the signals $S_{XA} = 1$, $S_{Xa} = 0$, $S_{YA} = 0$, and $S_{Ya} = 1$. Besides, since String X will be connected to the grid terminal, then the voltage to be synthesized across String X becomes equal to the grid voltage reference ($v^*_{sX} = v^*_{ga}$) and the String-X current becomes equal to the grid current ($i_X = i_{ga}$). Finally, since String Y will be connected to the generator terminal, then the voltage to be synthesized across String Y becomes equal to the generator voltage reference ($v^*_{sY} = v^*_{la}$) and the String-Y current becomes equal to the generator current ($i_Y = i_{la}$).

After defining the voltage references and currents of the two strings, the next step is the String-X and String-Y control. Taking String X as an example for the explanation, the first step of the control is the modulation. In this paper, a level-shifted-carrier pulse-width modulation (LSC-PWM) technique is adopted. The modulation block receives as an input the String-X voltage reference (v^*_{sX}) and it provides as an output the instantaneous number of submodules to be inserted (Z) in order to track the voltage reference. The flowchart shown in Fig. 9 explains how the hybrid MMShC was controlled to obtain the simulation results shown in Fig. 8. This flowchart is interesting because it explains the converter control in a didactic and intuitive way. However, the flowchart only explains partially the converter control for the specific operation condition of the simulation results shown in Fig. 8. The complete control would not be possible

to be represented in such a figure. Nonetheless, the explanation of the complete control will be provided later in this paper. So, since in the simulation, whose results are shown in Fig. 8, the power supplied to the grid was higher than the power absorbed by the WT, then if String X were connected to the generator terminal, then no battery submodule had to be inserted. On the contrary, if String X were connected to the grid terminal, then battery submodules had to be inserted. The signal *tri* is the one that defines the bidirectional-switch valves operation and, thus, defines the connection of the submodule string. Then, according to Fig. 9, if *tri* is bigger than 0.5, then String X will be connected to the generator terminal and, thus, only capacitor submodules must be inserted, i.e., $N_{cap} = Z$ and $N_{bat} = 0$. If *tri* is smaller than 0.5, however, then battery submodules must be inserted. The variable *auxX* was initialized with a value equal to 0. The control algorithm will test if $auxX = 0$, which will be true in the first time the code is read. Thus, the code will start in the left-hand side of the *if* statement. This condition corresponds to the situation in which the average value of the submodule-capacitor voltages are increasing as illustrated in Fig. 8(e) and (f). So, while the submodule capacitor voltages (v_{AX1}) remain smaller than the upper limit ($L_{up} = 1.1$ kV), the submodule insertion pattern is the following: if $Z \leq 1$, then $N_{cap} = 0$ and $N_{bat} = Z$. If $Z > 1$, then $N_{cap} = Z - 1$ and $N_{bat} = 1$. This means that one battery submodule must always be inserted when Z is at least equal to 1. Once again, during this period the submodule-capacitor voltages are increasing since the power supplied by the batteries to the grid is higher than the power mismatch between P_g and P_l. When the submodule-capacitor voltages exceed the upper limit ($L_{up} = 1.1$ kV), then the insertion pattern becomes the following: $N_{cap} = Z$ and $N_{bat} = 0$ and the variable *auxX* assumes a value equal to 1. Now, only capacitor submodules will be inserted when String X is connected to the grid. Thus, the average value of the submodule-capacitor voltages starts to decrease, since the capacitors are discharged at a higher rate when connected to the grid terminals than they are charged when connected to the WT terminals. Since now $auxX = 1$, then the code will enter the right-hand side of the *if* statement. In this case, while the submodule-capacitor voltage (v_{AX1}) remains bigger than the lower limit ($L_{low} = 0.9$ kV), then the insertion pattern is the following: $N_{cap} = Z$ and $N_{bat} = 0$. When the submodule-capacitor voltages exceed the lower limit ($L_{low} = 0.9$ kV), then the insertion pattern becomes the following: if $Z \leq 1$, then $N_{cap} = 0$ and $N_{bat} = Z$. If $Z > 1$, then $N_{cap} = Z - 1$ and $N_{bat} = 1$. Moreover, the variable *auxX* assumes a value equal to 0. Now, the average value of the submodule-capacitor voltages starts to increase again, since battery submodules are inserted. The control remains operating between these two states and, thus, the submodule-capacitor voltages remain regulated within the upper and lower limits ($L_{up} = 1.1$ kV and $L_{low} = 0.9$ kV, respectively).

The previously explained stage of the control was responsible for defining the instantaneous number of capacitor submodules (N_{cap}) and battery submodules (N_{bat}) to be inserted. The next step is the sorting algorithm that decides, which of the N available capacitor submodules and which of the M available battery submodules of the string should be inserted. The sorting algorithm aims to maintain all the capacitors within the same string with similar voltage values and all the batteries within the same string with similar SOC values. The sorting algorithm basically checks the polarity of the submodules to be inserted (which is equal to the polarity of the voltage reference v^*_{sX}) and it checks the instantaneous direction of the current (if i_X has a positive or a negative value). Depending on the combination of voltage polarity and current direction, this current will be charging or discharging the capacitors and batteries of the inserted submodules. If this is a charging current, then the N_{cap} submodules with lower capacitor voltage values and the N_{bat} submodules with lower battery SOC values are selected to be inserted. On the contrary, if this is a discharging current, then the N_{cap} submodules with higher capacitor voltage values and the N_{bat} submodules with higher battery SOC values are selected to be inserted. With this algorithm, all the capacitors within the same string remain with similar voltage values and all the batteries within the same string remain with similar SOC values as demonstrated in Fig. 7. Finally, the N_{cap} selected capacitor submodules and the N_{bat} selected battery submodules are inserted.

The complete hybrid-MMShC control algorithm would require as an input the power values P_g and P_l since if $P_g > P_l$, then battery submodules would have to be inserted in the strings connected to the grid to inject the surplus power into the grid. On the contrary, if $P_l > P_g$, then battery submodules would have to be inserted in the strings connected to the generator to absorb the surplus power produced by the WT. Besides, different voltage limits would be required to define the number of battery submodules to be inserted to maintain the capacitor voltages regulated, as illustrated in Fig. 10 and Fig. 11.

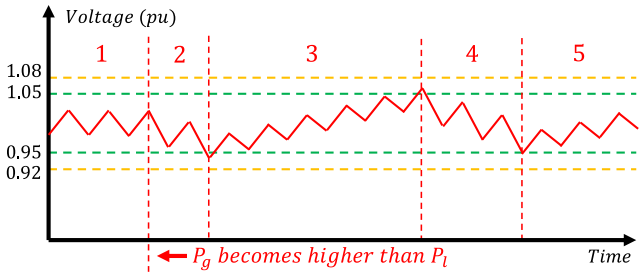

FIGURE 10. Submodule-capacitor voltages.

Let us consider the example shown in Fig. 10. Initially (interval 1), the power injected into the grid by the hybrid MMShC (P_g) is equal to the power absorbed from the WT (P_l) and, thus, the average value of the submodule capacitor voltages is kept regulated at the nominal value equal to 1 pu. At the beginning of interval 2, the power injected into the grid becomes higher than the power produced by the WT

and, thus, the average value of the submodule-capacitor voltages starts to decrease since only capacitor submodules are inserted at the grid terminals. In other words, the submodule insertion pattern of the strings connected to the grid, during interval 2, is: if the submodule string is connected to the grid terminal, then $N_{cap} = Z$ and $N_{bat} = 0$. As soon as the submodule-capacitor voltages reach the first lower limit $L_{low1} = 0.95$ pu (represented by a dashed green line), then the submodule insertion pattern changes to insert one battery submodule in the strings connected to the grid. In other words, the insertion pattern becomes: if the submodule string is connected to the grid, then if $Z \leq 1$, then $N_{cap} = 0$ and $N_{bat} = Z$, and if $Z > 1$, then $N_{cap} = Z - 1$ and $N_{bat} = 1$. This is the beginning of interval 3. In this example, the insertion of only one battery submodule is enough to make the submodule-capacitor voltages to increase, which means that the power supplied by the batteries are higher than the mismatch between P_g and P_l. The submodule-capacitor voltages increase until they reach the first upper limit $L_{up1} = 1.05$ pu (represented by a dashed green line). As soon as the submodule-capacitor voltages reach the first upper limit, the insertion pattern goes back to: if the submodule string is connected to the grid terminal, then $N_{cap} = Z$ and $N_{bat} = 0$. Thus, the submodule-capacitor voltage starts to decrease again, which corresponds to interval 4. Finally, interval 5 is exactly the same as interval 3 and the control stays switching between these two stages until a new power mismatch between P_g and P_l occurs.

Let us now consider the example illustrated in Fig. 11. In this example, intervals 1 and 2 are exactly the same as intervals 1 and 2 of the previous example shown in Fig. 10. In other words, in interval 2, the average value of the submodule-capacitor voltage decreases, since $P_g > P_l$, and the submodule insertion pattern is: if the submodule string is connected to the grid terminal, then $N_{cap} = Z$ and $N_{bat} = 0$. However, in this example, the power injected into the grid is higher than the power injected into the grid in the previous example, which means that the power mismatch between P_g and P_l is higher. So, as soon as the submodule-capacitor voltages reach the first lower limit ($L_{low1} = 0.95$ pu), the submodule insertion pattern becomes: if the submodule string is connected to the grid, then if $Z \leq 1$, $N_{cap} = 0$ and $N_{bat} = Z$, and if $Z > 1$, $N_{cap} = Z - 1$ and $N_{bat} = 1$. However, in this case, the power injected into the grid by the batteries is still lower than the power mismatch between P_g and P_l, which means that the average value of the submodule capacitor voltages will continue to decrease but with a lower rate. This condition corresponds to interval 3 of Fig. 11. As soon as the submodule-capacitor voltages reach the second lower limit $L_{low2} = 0.92$ pu (represented by a dashed orange line), the submodule insertion pattern changes to insert one more battery submodule in the strings connected to the grid. In other words, the insertion pattern becomes: if the submodule string is connected to the grid, then if $Z \leq 2$, $N_{cap} = 0$ and $N_{bat} = Z$, and if $Z > 2$, $N_{cap} = Z - 2$ and $N_{bat} = 2$. Now, the power injected into the grid by the batteries becomes higher than the power mismatch between P_g and P_l and, thus, the average value of the submodule-capacitors starts to increase. This condition corresponds to interval 4 of Fig. 11. It is clear, now, that the conditions to make the submodule-capacitor voltages to increase and decrease (for this specific power mismatch between P_g and P_l) corresponds to the insertion of two battery submodules and of one battery submodule, respectively. Thus, as soon as the submodule-capacitor voltages reach the first upper limit ($L_{up1} = 1.05$ pu), the submodule insertion pattern comes back to: if the submodule string is connected to the grid, then if $Z \leq 1$, $N_{cap} = 0$ and $N_{bat} = Z$, and if $Z > 1$, $N_{cap} = Z - 1$ and $N_{bat} = 1$. So, the submodule-capacitor voltages start to decrease once again, which corresponds to interval 5 of Fig. 11. Finally, it is important to emphasize that, since the two states between which the control needs to switch are already known, then as soon as the submodule-capacitor voltages reach the first lower limit ($L_{low1} = 0.95$ pu), the insertion pattern becomes again: if the submodule string is connected to the grid, then if $Z \leq 2$, $N_{cap} = 0$ and $N_{bat} = Z$, and if $Z > 2$, $N_{cap} = Z - 2$ and $N_{bat} = 2$. This condition corresponds to interval 6 of Fig. 11.

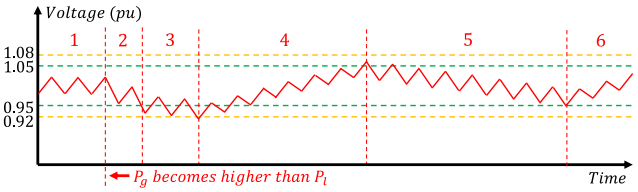

FIGURE 11. Submodule-capacitor voltages.

The examples illustrated in Fig. 10 and in Fig. 11 only consider the cases in which $N_{bat} = 1$ and $N_{bat} = 2$. However, in practice, more limits would be required to account for the cases in which more battery submodules would have to be inserted. Another possible approach would be to estimate the number of battery submodules to be inserted based on the power mismatch between P_g and P_l and based on the calculation of the battery power. In other words, by knowing the instantaneous battery current and the battery voltage, it would be possible to calculate the amount of power charging/discharging the batteries and, then it would be possible to estimate how many battery submodules would have to be inserted to absorb/supply the surplus power between P_g and P_l. This approach will be analyzed in future works.

IV. CONCLUSION

This paper introduced an enhanced version of the recently presented MMShC with integrated energy storage, which could be suitable to drive modern/future high-power medium-voltage WTs. The enhanced converter proposed in this paper is a hybrid topology in which the submodule strings are composed of a combination of battery submodules and of capacitor submodules. In this paper, a control technique was

proposed to regulate the submodule-capacitor voltages of the converter by controlling the insertion of battery submodules, while allowing for the dispatchable operation of the WT. In other words, a given number of battery submodules had to be inserted depending on the mismatch between the power produced by the WT and the power to be injected into the grid, in a way to preserve the balance between the power charging the converter capacitors when connected to the generator terminals and the power discharging these capacitors when connected to the grid terminals.

Simulation results were presented, which demonstrated the dispatchable operation as the proposed solution injected into the grid a power value different from the power instantaneously generated by the turbine. These results proved that the conventional capacitors, implemented into the converter, were the ones responsible for transferring the power generated by the WT to the grid, and the submodule batteries only had to handle either the surplus power generated by the turbine or the extra power required to be injected into the grid. In Fig. 6, simulation results demonstrated the operation of the converter with capacitors only while the turbine operated in a dispatchable mode. These results showed that the average value of the capacitor voltages varied along the simulation since a different power value was injected into the grid in relation to the power generated by the turbine, in a way that the capacitors were discharged with a different rate when connected to the grid terminals than they were charged when connected to the generator terminals. In Fig. 7, however, simulation results were presented in which some battery submodules were inserted to preserve the balance between the power charging the capacitors of the strings connected to the generator and the power discharging the capacitors of the strings connected to the grid. This way, the submodule-capacitor voltages were kept constant and regulated throughout the simulation. However, the results shown in Fig. 7 corresponded to an ideal case where the power absorbed/supplied by the inserted batteries was exactly equal to the difference between the power instantaneously produced by the WT and the power instantaneously injected into the grid. Thus, in Fig. 8, simulation results were presented demonstrating the real operation of the converter in which the multiple limits explained in Fig. 10 and Fig. 11 had to be used to perform the submodule-capacitor voltage regulation.

The hybrid topology presented in this paper should be more cost effective than the original one (with batteries handling the full turbine power) since the dimensions of the battery system could be reduced and these batteries would have a longer lifetime. The following are important issues to be analyzed in future works:

- Study the possibility of enhancing the control algorithm by implementing the decision-making process of the required number of battery submodules to be inserted based on the calculation/estimation of the battery power instead of based on the multiple upper/lower limits explained in Fig. 10 and in Fig. 11.
- Develop a cost analysis of the proposed hybrid solution in relation to the original topology with batteries only, as well as in relation to other well-established approaches to integrate an ESS into wind power plants, as for example the usage of an extra converter exclusively dedicated to the ESS.
- Present experimental results based on a low-scale prototype of the proposed topology to further validate it.

REFERENCES

[1] M. Diaz, R. Cardenas, M. Espinoza, A. Mora, and P. Wheeler, "Modelling and control of the modular multilevel matrix converter and its application to wind energy conversion systems," in *Proc. 42nd Annu. Conf. Ind. Electron. SoC.*, Florence, Italy, Oct. 2016, pp. 5052–5057.
[2] N. Fichaux *et al.*, "UPWIND—Design limits and solutions for very large wind turbines," Eur. Wind Energy Assoc., Brussels, Belgium, Tech. Rep., 2011.
[3] M. Diaz, R. Cardenas, M. Espinoza, F. Rojas, A. Mora, J. C. Clare, and P. Wheeler, "Control of wind energy conversion systems based on the modular multilevel matrix converter," *IEEE Trans. Ind. Electron.*, vol. 64, no. 11, pp. 8799–8810, Nov. 2017.
[4] A. Madariaga, J. L. Martín, I. Zamora, I. M. de Alegría, and S. Ceballos, "Technological trends in electric topologies for offshore wind power plants," *Renew. Sustain. Energy Rev.*, vol. 24, pp. 32–44, Aug. 2013.
[5] *PCS 6000 for Large Wind Turbines Medium Voltage, Full Power Converters Up to 9 MVA*, ABB, Zürich, Switzerland, 2012.
[6] J. Esch, "High-power wind energy conversion systems: State-of-the-art and emerging technologies," *Proc. IEEE*, vol. 103, no. 5, pp. 736–739, May 2015.
[7] L. Qu and W. Qiao, "Constant power control of DFIG wind turbines with supercapacitor energy storage," *IEEE Trans. Ind. Appl.*, vol. 47, no. 1, pp. 359–367, Jan. 2011.
[8] L. Miao, J. Wen, H. Xie, C. Yue, and W.-J. Lee, "Coordinated control strategy of wind turbine generator and energy storage equipment for frequency support," *IEEE Trans. Ind. Appl.*, vol. 51, no. 4, pp. 2732–2742, Jul. 2015.
[9] F. D. González, F. D. Bianchi, A. Sumper, and G. O. Bellmunt, "Control of a flywheel energy storage system for power smoothing in wind power plants," *IEEE Trans. Energy Convers.*, vol. 29, no. 1, pp. 204–214, Mar. 2014.
[10] D. Pagnani, F. Blaabjerg, C. L. Bak, F. M. Faria da Silva, L. H. Kocewiak, and J. Hjerrild, "Offshore wind farm black start service integration: Review and outlook of ongoing research," *Energies*, vol. 13, no. 23, p. 6286, Nov. 2020.
[11] P. Pinson, "Wind energy: Forecasting challenges for its operational management," *Stat. Sci.*, vol. 28, no. 4, pp. 564–585, Nov. 2013.
[12] S. K. Chaudhary, A. F. Cupertino, R. Teodorescu, and J. R. Svensson, "Benchmarking of modular multilevel converter topologies for ES-STATCOM realization," *Energies*, vol. 13, no. 13, p. 3384, Jul. 2020.
[13] M. Vasiladiotis and A. Rufer, "Analysis and control of modular multilevel converters with integrated battery energy storage," *IEEE Trans. Power Electron.*, vol. 30, no. 1, pp. 163–175, Jan. 2015.
[14] N. Kawakami, S. Ota, H. Kon, S. Konno, H. Akagi, H. Kobayashi, and N. Okada, "Development of a 500-kW modular multilevel cascade converter for battery energy storage systems," *IEEE Trans. Ind. Appl.*, vol. 50, no. 6, pp. 3902–3910, Nov. 2014.
[15] J. I. Y. Ota, T. Sato, and H. Akagi, "Enhancement of performance, availability, and flexibility of a battery energy storage system based on a modular multilevel cascaded converter (MMCC-SSBC)," *IEEE Trans. Power Electron.*, vol. 31, no. 4, pp. 2791–2799, Apr. 2016.
[16] B. Novakovic and A. Nasiri, "Modular multilevel converter for wind energy storage applications," *IEEE Trans. Ind. Electron.*, vol. 64, no. 11, pp. 8867–8876, Nov. 2017.
[17] G. F. Gontijo, T. Kerekes, D. Sera, M. Ricco, L. Mathe, and R. Teodorescu, "Medium-voltage converter solution with modular multilevel structure and decentralized energy storage integration for high-power wind turbines," *IEEE Trans. Power Electron.*, vol. 36, no. 11, pp. 12954–12967, Nov. 2021.
[18] D. Sera, L. Mathe, and M. Ricco, "Flexible and efficient switched string converter," U.S. Patent WO 2020 043 258 A1, Mar. 5, 2020.
[19] F. Zhao, X. Wang, Z. Zhou, L. Harnefors, J. R. Svensson, U. H. Kocewiak, and M. P. S. Gryning, "Control interaction modeling and analysis of grid-forming battery energy storage system for offshore wind power plant," *IEEE Trans. Power Syst.*, early access, Jul. 14, 2021, doi: 10.1109/TPWRS.2021.3096850.

[20] J. Khazaei, D. H. Nguyen, and A. Asrari, "Consensus-based demand response of PMSG wind turbines with distributed energy storage considering capability curves," *IEEE Trans. Sustain. Energy*, vol. 11, no. 4, pp. 2315–2325, Oct. 2020.
[21] F. V. Robinson and V. Hamidi, "Series connecting devices for high-voltage power conversion," in *Proc. 42nd Int. Univ. Power Eng. Conf.*, Sep. 2007, pp. 1134–1139.
[22] K. Sharifabadi, L. Harnefors, H.-P. Nee, S. Norrga, and R. Teodorescu, *Design, Control, and Application of Modular Multilevel Converters for HVDC Transmission Systems*. Hoboken, NJ, USA: Wiley, 2016.

GUSTAVO F. GONTIJO (Member, IEEE) received the B.Sc. and M.Sc. degrees in electrical engineering from the Federal University of Rio de Janeiro (UFRJ), Rio de Janeiro, Brazil, in 2016 and 2018, respectively. He is currently pursuing the Ph.D. degree with the AAU Energy, Aalborg University, Aalborg Øst, Denmark.

From 2014 to 2015, he was an Intern with the Leopoldo Americo Miguez de Mello Research and Development Center (Cenpes), Brazilian Energy Company Petrobras, where he was involved with research works about solar photovoltaic systems and wind turbines. From 2015 to 2019, he was with the Laboratory of Power Electronics and Medium Voltage Applications, which is part of the Alberto Luiz Coimbra Institute for Graduate Studies and Research in Engineering (COPPE/UFRJ). From 2020 to 2021, he was a Research Assistant with the AAU Energy, Aalborg University. He is currently a Guest Researcher with Ørsted A/S, Gentofte, Denmark, where he is working in a research collaboration with the title "Eigenvalue-Based Stability Assessment of Offshore Wind Power Plants with MMC-Based HVDC Connection." His current research interests include modular multilevel converter solutions with and without energy-storage integration for medium-voltage applications, stability of power-electronic-based power systems, modern HVDC transmission systems based on the modular multilevel converter, power electronic solutions and control techniques applied to AC/DC microgrids, and power electronic solutions to improve the power quality of wind turbines.

DEZSO SERA (Senior Member, IEEE) received the B.Sc. and M.Sc. degrees in electrical engineering from the Technical University of Cluj, Romania, in 2001 and 2002, respectively, and the M.Sc. degree in power electronics and the Ph.D. degree in PV systems from the AAU Energy, Aalborg University (AAU), Denmark, in 2005 and 2009, respectively.

From 2010 to 2019, he was the Leader of the Photovoltaic Systems Research Program, AAU. He joined the Queensland University of Technology (QUT), Brisbane, Australia, as an Associate Professor, in 2020. He is currently the Deputy Director and a Program Leader of the Centre for Clean Energy Technologies and Practices, QUT. His research interests include modeling, characterization, diagnostics and maximum power point tracking (MPPT) of PV arrays, as well as power electronics and grid and energy storage integration for PV systems.

MATTIA RICCO (Senior Member, IEEE) received the master's degree *(cum laude)* in electronic engineering from the University of Salerno, Fisciano, Italy, in 2011, and the dual Ph.D. degree in electrical and electronic engineering from the University of Cergy–Pontoise, Cergy–Pontoise, France, and in information engineering from the University of Salerno, in 2015. From 2015 to 2018, he was a Postdoctoral Research Fellow with AAU Energy, Aalborg University, Denmark. Since December 2018, he has been a Senior Assistant Professor (Tenure Track) with the Department of Electrical, Electronic, and Information Engineering, University of Bologna, Bologna, Italy. His research interests include modular multilevel converters, battery management systems, electric vehicle chargers, field-programmable gate array-based controllers, identification algorithms for power electronics, and photovoltaic systems.

LASZLO MATHE (Senior Member, IEEE) received the B.Sc. and M.Sc. degrees in electrical engineering from the Technical University of Cluj-Napoca, Cluj-Napoca, Romania, in 2000 and 2002, respectively, and the Ph.D. degree in electrical engineering from the AAU Energy, Aalborg University, Aalborg, Denmark, in 2010. From 2002 to 2007, he worked with the industry as a Control Development Engineer. From 2007 to 2017, he worked as a Ph.D. Fellow, an Assistant, and finally as an Associate Professor at Aalborg University. Since 2017, he has been working as a Motor Control Expert at Robert Bosch Company. His current research interests include control and design of power converters, control of electrical drives, photovoltaic systems, modulation techniques (MMC, two level inverters), and vehicle electrification.

TAMAS KEREKES (Senior Member, IEEE) received the Engineering Diploma degree with specialization in electric drives and robots from the Technical University of Cluj-Napoca, Cluj-Napoca, Romania, in 2002, and the M.Sc. degree in power electronics and drives and the Ph.D. degree in analysis and modeling of transformerless PV inverter systems from the AAU Energy, Aalborg University, Aalborg, Denmark, in 2005 and 2009, respectively.

He is currently an Associate Professor with the AAU Energy, Aalborg University, doing research in the field of grid-connected renewable applications. His research interests include grid-connected applications based on dc–dc, dc–ac single- and three-phase converter topologies focusing also on switching and conduction loss modeling and minimization in the case of Si and new wide bandgap devices.

REMUS TEODORESCU (Fellow, IEEE) received the Dipl.Ing. degree in electrical engineering from the Politehnica University of Bucharest, Romania, in 1989, and the Ph.D. degree in power electronics from the University of Galati, Romania, in 1994.

In 1998, he joined the Power Electronics Section, AAU Energy, Aalborg University, where he currently works as a Full Professor. From 2013 to 2017, he was a Visiting Professor with the Chalmers University of Technology, Sweden. He has coauthored the books *Grid Converters for Photovoltaic and Wind Power Systems* (Wiley-IEEE Press, 2011) and *Design, Control and Application of Modular Multilevel Converters for HVDC Transmission Systems* (Wiley-IEEE Press, 2016). He has coauthored over 500 IEEE journal articles and conference papers. His research interests include design and control of grid connected converters for photovoltaic and wind power systems, HVDC/FACTS based on MMC, SiC-based converters, storage systems for utility based on Li-Ion battery technology, and battery lifetime model using artificial intelligence. In 2021, he was awarded the Villum Investigator grant for the development of the Center of Research on Smart Battery at Aalborg University.